RSC Advances

ROYAL SOCIETY OF CHEMISTRY

www.rsc.org/advances

Journal Name

COMMUNICATION

High-Performance Supercapacitors Based on Electrospun Multichannel Carbon Nanofibers

Received 00th January 20xx,
Accepted 00th January 20xx

DOI: 10.1039/x0xx00000x

www.rsc.org/

Lijuan Zhang[a, b], Linlin Han[a, b], Shuai Liu[a, b], Cui Zhang[a, b, *], Shuangxi Liu[a, b, *]

Multichannel carbon nanofibers (MCNFs) have been fabricated by annealing electrospun PAN/PS immiscible polymers nanofibers. The obtained mechanically flexible mats of MCNFs, possessing integrative architecture, are used as electrode directly no binder and without any activated process. Owing to the binder-free characteristic, unique multichannel structure and high specific surface area, the MCNFs perform high capacitance (270 F g^{-1} at the current density of 0.5 A g^{-1}), perfect cycling stability (the capacitance no decrease after 5000 cycles at the current density of 1 A g^{-1}), excellent rate capability (89% retention at the current density of 20 A g^{-1}) and high energy and power density. These results demonstrate that the electrode material has a promising prospect on applications of energy storages.

Supercapacitors, possessing a high power density and long cycle life, have been wildly used in various areas such as electric vehicles, memory back-up, power quality management, battery improvement and renewable energy applications.[1,2] Various typical electrode materials have been studied including carbon materials, metal oxides and conducting polymers.[3,4] Compared with metal oxides and conducting polymer, carbon electrodes have high electric conductivity, long cycle life and stable physicochemical properties. For example, graphene, carbon nanotubes, activated carbon, carbon aerogels, highly porous carbon and porous carbon nanofibers (PCNFs) have attracted great attention.[5-11] Among these carbon materials, one-dimensional (1D) PCNFs play an important role owing to high conductivity, chemical stability and more importantly 1D structure with tunable high specific surface area (SSA) and excellent capacitance performance.[12,13] Electrospinning, as one of the most important method for preparing 1D nanomaterials, has attracted wide research interests in recent years.[14,15] Also, Electrospinning is low-cost, facile and versatile method which can be designed to fabric PCNFs with high SSA. It is well-known that SSA impacts on capacitance performance of PCNFs as suprecapacitor.[16,17] Given this, various activation methods are used to carbon nanofiber materials for increasing SSA. For instance, using CO_2 and KOH as activation in post-processing or incorporating KOH in as-spun nanofibers as porogenic agent and activator.[18-20] These activation methods are very effective process to improve the SSA of carbon materials, but it is inevitable to increase the workload in experiments. In addition, this process also destroys integrative architecture of the carbon nanofiber mat. The integrative electrode materials, as binder-free electrodes, are beneficial to increase the conductivity and reduce the ion transport resistance in electrochemical behaviors.[21] Therefore, it is highly desirable to simplify experiment and prepare integrative binder-free electrodes which possess high SSA.

Herein, to solve the above-mentioned problem, we prepare a kind of unique structure PCNFs possessing multi-channel and high SSA by electrospun immiscible PAN/PS polymer blends followed by thermal treatments of pyrolysis, stabilization and carbonization (Scheme 1). The obtained materials are named as multichannel carbon nanofibers (MCNFs). This material supplies ion-transport channel in the internal to induce the ion-diffusion insistence. In addition, the obtained MCNFs don't need activation, so it still keeps integrative for being used as binder-free electrode material. Benefiting from the multichannel structure and binder-free electrode, the MCNFs exhibit excellent capacitance performance with significantly improved specific capacitance, outstanding rate capability and high power density.

Polyacrylonitrile (PAN, Mw=80000) was purchased from Kunshan plastic Co., Ltd. Polystyrene (PS, Mw=260000) was purchased from Aladdin. N, N-Dimethylformamide (DMF, C_3H_7NO, AR, 99.5%) was purchased from Aladdin. Regents and materials are analytical grade and used without any further purification.

The electrospinning precursor was prepared by dissolving PS 8 wt% and PAN 5 wt% in DMF solvent. This solution was then stirred continuously for 24 h before spinning. During

[a] Institute of New Catalytic Materials Science, School of Materials Science and Engineering, Nankai University, Tianjin 300071, PR China
[b] bTianjin Collaborative Innovation Center for Chemistry & Chemical Engineering, Tianjin 300071, PR China.

*Corresponding author. Tel./fax: +86 22 23509005.
E-mail address: sxliu@nankai.edu.cn (S. Liu), zhangcui@nankai.edu.cn (C. Zhang)

Electronic Supplementary Information (ESI) available: [details of any supplementary information available should be included here]. See DOI: 10.1039/x0xx00000x

electrospinning, the precursor solution was set in a syringe to yield a stable Taylor cone under the flow rate of 0.5 ml h^{-1}. A

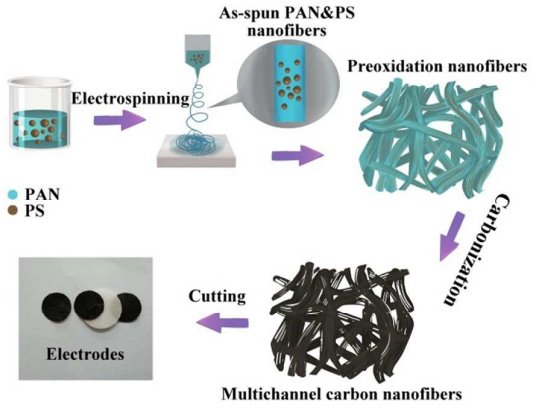

Scheme 1. Schematic illustration of the synthesis process for MCNFs

voltage-supply wire was attached to the charging needle and applied voltage is 15 kV. The distance from the needle tip to the fiber collector was 18 cm. The as-spun fibers were stabilized at 250 ℃ for 2 h in the tube furnace under air circumstance at the heating rate of 5 ℃ min^{-1}. This step taking an important effect was to cross-link PAN chains and prepared a structure that could withstand rigors of high temperature processing subsequently.[22] Meanwhile, the PS in blend fibers began to decompose. With the temperature increasing, PS was removed forming abundant channels in the PAN carbon nanofibers at the 800 ℃ for 2 h thermal treatment in N_2 atmosphere. The MCNFs were obtained.

The surface morphology and microstructure of MCNFs were characterized by field emission scanning electron microscopy (FESEM JSM-7500F) at 5 kV. The transmission electron microscopy (TEM) images were obtained by Tecnai-F20 system operated at 200 kV. X-ray diffraction (XRD) pattern was obtained from ground-up samples of MCNFs using a Bruker D8 FOCUS diffractormeter and Cu Kα (λ=0.15418). Raman spectrum was recorded by Renishaw inVia with a wavelength of 514 nm to calculate the degree of crystallinity. The surface chemical composition was examined by X-ray photoelectron spectroscopy (XPS). The surface areas and the pore structures were measured using a Tristar 3000 surface area and pore analyzer. The pore size distributions were calculated using the BJH method.

Electrochemical performance was detected on a CHI 660D electrochemical workstation by 2-electrode method (the typical symmetrical coin cell). The electrodes were obtained by cutting the as-prepared MCNFs mat into disk shapes (diameter: 12 mm; thickness: 200μm) without any conductive additives and no binder. Two pieces of nearly equal weight MCNF electrode were separated by separator. Before electrochemical measurements, the electrodes and separator were immersed in electrolyte solution of 6M KOH under vacuum in order to make them full immersion. The electrochemical behaviors of samples included cyclic voltammetry (CV) and electrochemical impedance spectroscopy (EIS) were detected on a CHI 660D electrochemical workstation. The test of galvanostatic charge-discharge (GCD) was studied using LAND CT2001A instrument. The capacitance of the supercapacitor cell of the carbon was calculated by the following equation:[23]

$$C = 2I \cdot \Delta t/(m \cdot \Delta V) \quad (1)$$

$$E = 1/8 \cdot C \cdot \Delta V^2 \quad (2)$$

$$P = E/\Delta t \quad (3)$$

Where *I* is the current (A), Δt is the discharge time (s), *m* is the mass of a single electrode (g), ΔV is the potential range (V). And *C*, *E*, and *P* indicate specific capacitance (F g^{-1}), average energy density (Wh kg^{-1}) and power density (W kg^{-1}).

Fig. 1 shows the morphology features of typical PAN/PS composite fibers and MCNFs in the SEM images, respectively. The PAN/PS composite nanofibers had a unified diameter and smooth surface (Fig. 1a). After carbonation, MCNFs are full of cracks on surface and the diameter of the fibers diminished slightly (Fig. 1b). The emerging of sunken indicates that multichannel structure had formed inside. It can be proved by the SEM photograph in Fig. 1d, which shows the details of the structure including sunken and multichannel characteristics on the images of sectional view. These characteristic structures are contributed to increase the SSA of the MCNFs and store most of the ion charges in the electrode and good capacitive behavior. It is obvious that the 1 dimension MCNFs overlap disorderly to form a multiplayer net structure to be fabricated into MCNF mat which have good mechanic strength and superior wettability to be used as binder-free electrode plate directly.

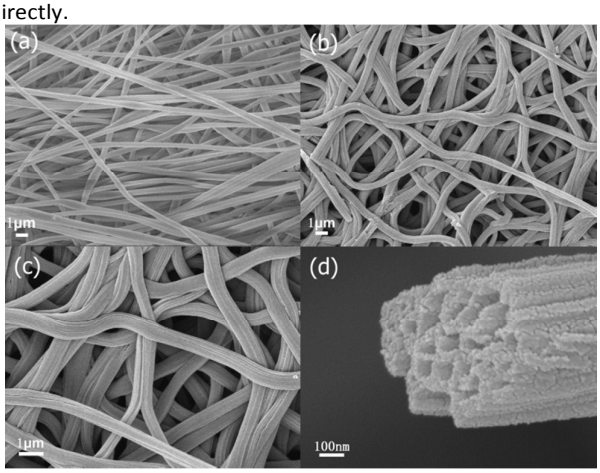

Fig. 1. SEM images: (a) PAN and PS nanofibers; (b) and (c) MCNFs at different magnification; (d) the cross section of MCNF.

As shown in Fig. 2, further details of the internal structure MCNF can be clearly observed by TEM. The high-resolution TEM images as inset in Fig. 2c displays the MCNFs are composed by the graphitic planner structure. And some visible channels accompanying scattered pores appear in the interior of MCNFs. The channel width of MCNF (Fig. 2d) display with the varying sizes including amount of evident mesopores width and inconspicuous micropores width. In addition, a plenty of micropores and mesopores are full of the walls of channels which play a double roles in storing ion charge and connecting

multi-channels. The unique structure of MCNF makes for ion transport and increase of capacitive performance.[24]

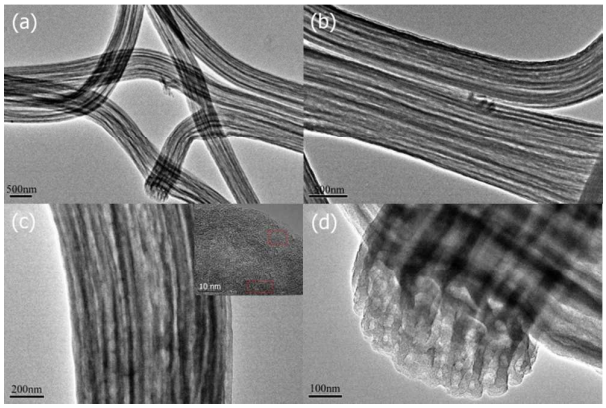

Fig. 2. TEM images of MCNFs (a), (b) and (c); inset shows the HRTEM image; the cross section of MCNF (d).

The XRD pattern of the MCNFs is shown in Fig. 3a, a broad peak around 24.7° can be attributed to (002) diffraction peak of turbostratic carbon, suggesting relatively low graphitization degree. The other diffraction peak at 43° is indexing to the (100) diffraction of carbon material with amorphous or disorder nature. [25]

In Fig. 3b, Raman spectra of the MCNFs showed D band at 1355 cm^{-1} and G band 1588 cm^{-1}, in which the G band demonstrates the in-plane vibration of the sp^2 carbon atoms, while the D band represents the disorder carbon or defective graphitic structure of the material. The integrated intensity ratio of D to G band (I_D/I_G) is 0.95 for the sample, suggesting the formation of turbostratic structure.

X-ray photoelectron spectrum (XPS) was used to study the surface composition of the MCNF. The wide scan XPS spectrum in Fig. 3c shows that the MCNF consists of C and O, peaking at the binding energies of around 284.6 eV and 533.8 eV. As show in Fig. 3d, the C1s XPS spectrum of MCNF can be fitted by three component peaks at binding energies of about 284.6, 285.7, and 288.8 eV, which may be respectively attributable to (C-C,C-O and C=O) species.[26] Therefore, there are some oxygen-contained functional groups derived from the carbonization of the PAN. These oxygen-enriched functionalities can both improve wettability and produce pseudocapacitance to bring about better supercapacitive performance.

The N_2 adsorption-desorption isotherms of the MCNFs (Fig. 4a) exhibit a combined characteristic of type Ⅳ isotherms with clear H2-type hysteresis loop, in which an obvious step increase in adsorption amount at very low relative pressure can be proved due to the existence of micropores. The existence of a hysteresis loop at medium P/P_0 indicates the presence of huge amount of mesopores. In addition, H2-type hysteresis loop which mainly represents typical "ʊ" pores and different diameter tubular pores is corresponding to internal structure of MCNF. The measured Brunauer-Emmett-Teller (BET) specific surface area is up to 750 $m^2 g^{-1}$. In fact the ideal EC electrode materials should have a hierarchical porous structure containing macropores (large than 50nm) for ion-buffering reservoir, mesopores for ion transporting and micropores for enhancement of charge storage.[27] Therefore, the MCNFs are desirable that the porous structure has an optional variation in pore size and pore size distribution.

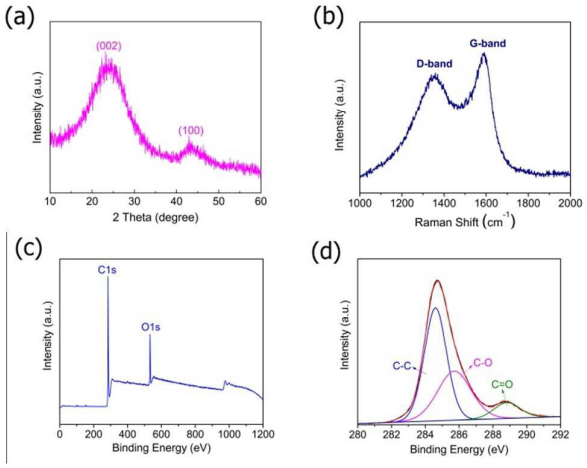

Fig. 3. (a) XRD pattern; (b) Raman spectrum; (c) XPS survey spectra; (d) XPS of C1s region.

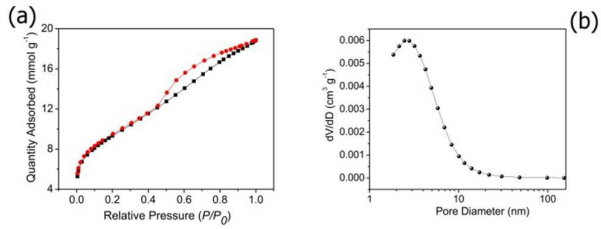

Fig. 4. (a) Nitrogen adsorption/desorption isotherm of MCNFs; (b) pore-size distribution of MCNFs calculated by BJH method.

Cyclic Voltammetry (CV) was used to evaluate the electrochemical performance of the MCNF electrodes. Fig. 5a shows the CV curves of the electrode at different scan rates from 5 mV s^{-1} to 200 mV s^{-1}. All the CV curves of the MCNF supercapacitors show almost rectangular shapes without obvious distortion even when the scan rate comes to 200 mV s^{-1}. Additionally, there exists a quick current response to the switching potential in the CV curves, indicating low equivalent series resistance, which can contribute to a high rate capability and power density.

Electrochemical impedance spectroscopy was employed to analyze the impedance behaviors of porous carbon materials. Fig. 5b displays the Nyquist plots of the supercapacitor using MCNF as electrode material, and the inset in the figure shows the semicircle is amplified at high frequency region of impedance. The semicircle represents the electrical resistance, corresponding to the equivalent series resistance (ESR) of the electrode which is quite crucial to the power density of the capacitor. The value of ESR obtained from the point intersecting with the real axis is only 0.42 Ω, which is lower than those reported in previous literatures.[28, 29] The oxygen-

containing groups, especially hydrophilic groups, on the surface can improve the wettability of the electrode and reduce the ESR. In the intermediate frequency region, a typical angle of 45° indicating a Warburg resistance is the characteristic of ion diffusion into the electrode interface. In the low frequency region, the Nyquist plots are nearly vertical which indicates a relatively ideal capacitive performance of the materials. This is the representative of the ion limiting diffusion process. These results demonstrate that porous structure of MCNF can promote the mass transfer or diffusion of ions into the pores effectively.

Galvanostatic charge-discharge (GCD) measurements were carried out to evaluate the rate performance of the MCNFs. The ability to retain high capacitance during fast charge-discharge processes is a crucial requirement for high performance and practical EDLCs. Fig. 5c shows the galcanostatic charge and discharge curves taken at different current densities in 6 M KOH in potential range from 0 to 1 V, and the charge-discharge curves exhibit almost symmetrical triangle and linear profiles at each current density, suggesting that it possesses an excellent double layer capacitive behavior. Fig. 5d draws the specific capacitances of MCNFs electrode corresponding to the different current densities. Overall, the MCNFs show a capacitance of 270 F g^{-1} at 0.5 A g^{-1} and 240 F g^{-1} (89% retention) when the current density increase to 20 A g^{-1}. This specific capacitance of the sample drops lightly with an increase in the current density of charge-discharge test, suggesting excellent rate capability profiting from the multichannel structure of electrode material.

Fig. 5e demonstrates the variation of specific capacitance with cycle number at 1 A g^{-1}. It can be seen from the plots that the specific capacitance of MCNFs presented no decrease after 5000 cycles even appeared a lightly increase comparing to the beginning, which indicates excellent electrochemical stability of the as-prepared MCNFs. In order to further confirm the outstanding capacitor performance of the MCNFs, the both energy and power densities are calculated and displayed in Fig. 5f. The energy density can reach as high as 9 Wh kg^{-1} at a power density of 0.12 kW kg^{-1} at 0.5 A g^{-1} and 3.1 Wh kg^{-1} at a power density of 3 kW kg^{-1} at 20 A g^{-1} which is higher than most of the previously reported carbon based symmetric supercapacitors in aqueous electrolytes.[30-35] Analysis shows that further improvements in energy and power density can be achieved by optimizing the nanoarchitecture of the electrodes

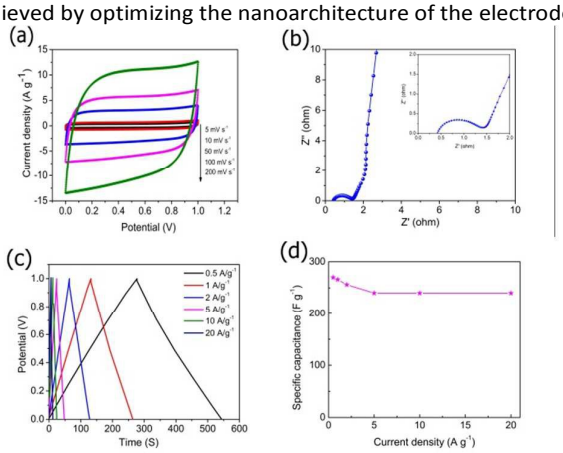

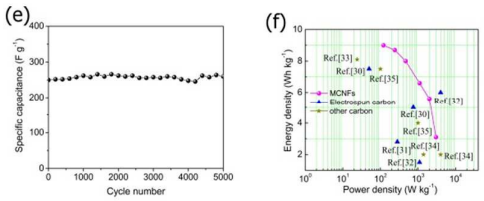

Fig. 5. (a) Cyclic voltammetry plots of MCNFs with different scan rates, (b) electrochemical impedance spectra of MCNFs as Nyquist polts, (c) and (d) charging-discharging curves and specific capacitances for MCNFs at different current densities, (e) specific capacitances for MCNFs at 1 A g^{-1} current density, (f) Ragone plots of the specific energy vs. specific power for MCNFs.

In this study, MCNFs are prepared by carbonizing the nanofibers of electrospinning PAN/PS blending precursor. The PS as sacrificial polymer is introduced into the PAN forming high SSA MCNFs without any activated process. The MCNFs have integrative architecture and can be used as binder-free electrodes to display outstanding capacitance performances. The electrochemical performances which are tested by symmetry supercapacitors show that the MCNFs possess high specific capacitance of 270 F g^{-1} at 0.5 A g^{-1} in 6 M KOH aqueous electrolyte, excellent cyclic stability and outstanding capacitance retention of 89% when the current density increased to 20 A g^{-1}. Noticeably, the E can reach 9 Wh kg^{-1} with P of 0.12 kW kg^{-1}, and the P is 3 kW kg^{-1} with E of 3.1 Wh kg^{-1}. These results exhibit that the MCNFs are not only wonderful electrode material for EDLC, but also have promising application in other energy storage devices.

Acknowledgements

These authors are grateful to the financial supported from National Natural Science Foundation of China (NNSFC 21003077) and Tianjin Natural Science Foundation, China (No.14JCZDJC32000) and MOE (IRT13R30).

References

1 P. Simon and Y. Gogotsi, Nat Mater, 2008, **7**, 845-854.
2 J. Sun, W. Li, B. Zhang, G. Li, L. Jiang, Z. Chen, R. Zou and J. Hu, Nano Energy, 2014, **4**, 56-64.
3 P. Hao, Z. Zhao, Y. Leng, J. Tian, Y. Sang, R. I. Boughton, C. P. Wong, H. Liu and B. Yang, Nano Energy, 2015, **15**, 9-23.
4 Z.-L. Wang, D. Xu, J.-J. Xu, L.-L. Zhang and X.-B. Zhang, Adv Funct Mater, 2012, **22**, 3699-3705.
5 B. C. Kim, H. T. Jeong, C. J. Raj, Y.-R. Kim, B.-B. Cho and K. H. Yu, Synthetic Met, 2015, **207**, 116-121.
6 J. Yan, T. Wei, Z. Fan, W. Qian, M. Zhang, X. Shen and F. Wei, J Power Sources, 2010, **195**, 3041-3045.
7 X. Cao, Y. Shi, W. Shi, G. Lu, X. Huang, Q. Yan, Q. Zhang and H. Zhang, Small, 2011, **7**, 3163-3168.
8 C. Nie, D. Liu, L. Pan, Y. Liu, Z. Sun and J. Shen, Solid State Ionics, 2013, **247–248**, 66-70.
9 W.-H. Qu, Y.-Y. Xu, A.-H. Lu, X.-Q. Zhang and W.-C. Li, Bioresource Technol, 2015, **189**, 285-291.
10 H. Chen, D. Liu, Z. Shen, B. Bao, S. Zhao and L. Wu, Electrochim Acta, 2015, 180, 241-251.

11 Z.-Y. Li, M. S. Akhtar and O. B. Yang, J Alloy Compd, 2015, **653**, 212-218.
12 J. Deng, T. Xiong, F. Xu, M. Li, C. Han, Y. Gong, H. Wang and Y. Wang, Green Chem, 2015, **17**, 4053-4060.
13. H.-G. Wang, S. Yuan, D.-L. Ma, X.-B. Zhang and J.-M. Yan, Energy & Environmental Science, 2015, **8**, 1660-1681.
14 C. H. Kim and B.-H. Kim, Electrochim Acta, 2014, **117**, 26-33.
15 S. Abouali, M. Akbari Garakani, B. Zhang, Z.-L. Xu, E. Kamali Heidari, J.-Q. Huang, J. Huang and J.-K. Kim, Acs Appl Mater Interfaces, 2015, **7**, 13503-13511.
16 T. Zhang, C. H. J. Kim, Y. Cheng, Y. Ma, H. Zhang and J. Liu, Nanoscale, 2015, **7**, 3285-3291.
17 Y. Gao, L. Li, Y. Jin, Y. Wang, C. Yuan, Y. Wei, G. Chen, J. Ge and H. Lu, Appl Energ, 2015, **153**, 41-47.
18 N. C. Abeykoon, J. S. Bonso and J. P. Ferraris, RSC Advances, 2015, **5**, 19865-19873.
19 C. Ma, Y. Song, J. Shi, D. Zhang, X. Zhai, M. Zhong, Q. Guo and L. Liu, Carbon, 2013, **51**, 290-300.
20 D. Lee, J.-Y. Jung, M.-J. Jung and Y.-S. Lee, Chem Eng J, 2015, **263**, 62-70.
21 H. He, L. Shi, Y. Fang, X. Li, Q. Song and L. Zhi, Small, 2014, **10**, 4671-4676.
22 N. Yusof and A. F. Ismail, J Anal Appl Pyrol, 2012, 93, 1-13.
23 C. Tran and V. Kalra, J Power Sources, 2013, **235**, 289-296.
24 Y. Han, S. Liu, D. Li and X. Li, Electrochim Acta, 2014, **138**, 193-199.
25 A. Sadezky, H. Muckenhuber, H. Grothe, R. Niessner and U. Pöschl, Carbon, 2005, **43**, 1731-1742.
26 M. Yang, Y. Zhong, J. Bao, X. Zhou, J. Wei and Z. Zhou, Journal of Materials Chemistry A, 2015, **3**, 11387-11394.
27 Y. Han, X. Dong, C. Zhang and S. Liu, J Power Sources, 2013, **227**, 118-122.
28 C. Lai, Z. Zhou, L. Zhang, X. Wang, Q. Zhou, Y. Zhao, Y. Wang, X.-F. Wu, Z. Zhu and H. Fong, J Power Sources, 2014, **247**, 134-141.
29 H. Luo, Y. Yang, X. Zhao, J. Zhang and Y. Chen, Electrochim Acta, 2015, **169**, 13-21.
30 T. Le, Y. Yang, Z. Huang and F. Kang, J Power Sources, 2015, **278**, 683-692.
31 Y. Dong, H. Lin, D. Zhou, H. Niu, Q. Jin and F. Qu, Electrochim Acta, 2015, **159**, 116-123.
32 E. J. Ra, E. Raymundo-Piñero, Y. H. Lee and F. Béguin, Carbon, 2009, **47**, 2984-2992.
33 F. Gao, G. Shao, J. Qu, S. Lv, Y. Li and M. Wu, Electrochim Acta, 2015, **155**, 201-208.
34 A. B. Fuertes and M. Sevilla, ChemSusChem, 2015, **8**, 1049-1057.
35 L.-F. Chen, Z.-H. Huang, H.-W. Liang, H.-L. Gao and S.-H. Yu, Adv Funct Mater, 2014, **24**, 5104-5111.

Graphic abstract

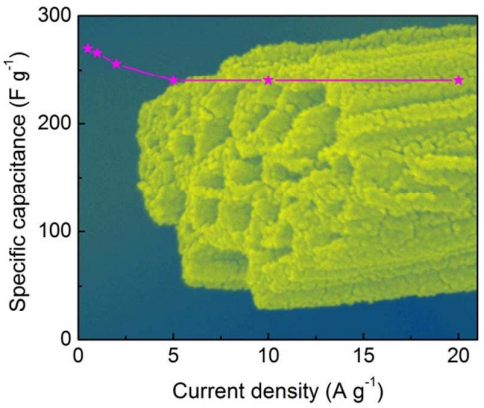

Multichannel carbon nanofibers exhibit high capacitance performance and excellent rate capability.